An Axisymmetric Nacelle and Turboprop Inlet Analysis Including Power Simulation

D. P. Golden,* T. J. Barber,† W. C. Chin‡
Pratt & Whitney Aircraft, East Hartford, Connecticut

An axisymmetric nacelle and turboprop inlet analysis is presented. The transonic small disturbance potential equation is solved in nonconservative form by means of column relaxation on a Cartesian mesh. Exact surface boundary conditions are implemented to account for the influence caused by the strong interatcion of neighboring bodies. The Kutta condition is included so that flow-through as well as sting mounted configurations can be simulated. The analysis includes an actuator disk model to simulate power input for either ducted fans or propellers. The actuator disk formulation specifies the necessary jump conditions both at the disk and along the jet plume or propeller wake slipstream. Comparisons are made with exact full potential solutions and with wind tunnel data.

Nomenclature

c = nacelle length
C_p = static pressure coefficient
K = transonic similarity parameter
M_∞ = freestream Mach number
$\dot{m}$ = mass flux
MFR = mass flow ratio
p = static pressure
q_∞ = freestream dynamic head
R_m = mean radius of nacelle
t = maximum thickness of nacelle
v = velocity vector
(x,r) = cylindrical coordinate system
γ = specific heat ratio
ϵ = R_m/c
ρ = density
τ = thickness ratio = t/c
ϕ = velocity potential
Φ = wake image point potential
[ ] = jump in included property

Subscripts

L = lower or inner wake flow
u = upper or outer wake flow
0 = stagnation state
∞ = freestream state

Introduction

THE inherent complexity of complete aircraft configurations renders largely impractical the purely experimental optimization of such systems, especially when operating in the transonic flow regime. Aside from being very expensive, it is often difficult or impossible to obtain the sort of detailed information which can be garnered from an analytic solution of the flowfield. The remarkable success of transonic flow analyses over relatively simple geometries which has been demonstrated in the past decade has encouraged the extension of the techniques to more complex configurations.

Some of the most successful three-dimensional aircraft simulations to date have been based on a small disturbance formulation and utilize Cartesian grids. Prominent examples are Boppe's[1,2] inclusion of pylon and powered nacelle effects, and Shankar and Malmuth's[3] inclusion of pylon and weapons stores effects. While the basic wing/body scheme has demonstrated reasonable agreement with test data, prediction of the influence of the nacelle and pylon has not been satisfactory. Thus there is still plenty of room for improvement even in the context of small disturbance theory.

This paper discusses several approaches at improving existing small disturbance formulations of nacelle/engine/aircraft interference effects. The question of nacelle modeling will be directly addressed with improvements to the basic slit boundary conditions and a more consistent formulation of the effects of power transfer for turbofan and turboprop application. A cylindrical Cartesian mesh is retained for its simplicity. Although conventional small disturbance theory assumes that improvements to slit boundary conditions are not warranted by the approximations in the governing equation, the results presented in this paper demonstrate that significant improvements can be obtained with little effort. This is especially important for extending the method to complicated three-dimensional geometries. Calculations using the various small disturbance methods will be presented and substantiated in cases where comparisons with full potential solutions and experimental data are possible.

Small Disturbance Formulation for Nacelles

Governing Equations

Most transonic methods for complex geometries apply small disturbance theory (SDT) to the governing equations, but frequently arrive at different model equations. Different models are obtained by considering alternate nondimensional scalings to identify the appropriate nonlinearities associated with a particular problem.[4] This approach can be complicated by the existance of multiple scalings.[5] The nacelle geometry is characterized by such a multiple limit process. The corresponding nacelle scale parameters are τ and ϵ.

In the limiting situation of $c/R_m \to 0$, the nacelle approaches an annular or ring wing limit, introduced by Kuchemann and Weber.[6] A scaling consistent thin wing theory

$$\epsilon \sim \tau^{2/3} \ll 1$$

$$K = (1-M_\infty^2)/\tau^{2/3} \cong 0(1)$$

reduces the potential equation to the Guderley-von Kármán

Presented as Paper 82-0256 at the AIAA 20th Aerospace Sciences Meeting, Orlando, Fla., Jan. 11-14, 1982; submitted Feb. 9, 1982; revision received Dec. 1, 1982.

*Engineer, Nacelle Aerodynamics Group.
†Research Engineer, Nacelle Aerodynamics Group. Member AIAA.
‡Supervisor, The Analysts, Schlumberger.

equation in cylindrical coordinates:

$$[(1-M_\infty^2)-(\gamma+1)M_\infty^2\phi_x]\phi_{xx}+\phi_{rr}+(1/r)\phi_r=0$$

$$r\phi_r(x,r\to R_m)=R_m(x)R_m'(x) \tag{1}$$

The outer and inner solutions are both consistent with Eq. (1). The alternative case of $R_m/c\to 0$, however, introduces additional considerations. The external solution reduces to the slender body limit when the scaling

$$\epsilon\sim\tau^2\ll 1$$

$$K=(1-M_\infty^2)/\tau^2\sim O(1)$$

is introduced and again Eq. (1) is retrieved. The internal flow, however, sees the centerline as an effective ground plane that, away from the leading edge, can be treated as a locally one-dimensional flow,[7] again consistent with Eq. (1).

Although a conservation form of Eq. (1) can be readily obtained, the model can be criticized for not being a proper small distrubance form of the mass conservation law[8]

$$\nabla\cdot[\rho(1+\phi_x)\bar{i}_x+\rho\phi_r\bar{i}_r]=0 \tag{2}$$

Perturbation equations which do have this property can be derived by properly truncating the series expansions for the mass flux components; for example,

$$\rho u\cong 1+(1-M_\infty^2)\phi_x-\tfrac{1}{2}[3-(2-\gamma)M_\infty^2]M_\infty^2\phi_x^2$$
$$-\tfrac{1}{2}[1-(2-\gamma)M_\infty^2]M_\infty^2\phi_x^3 \tag{3}$$

The present second-order expression is adequate for our purposes and, at transonic speeds, is reasonably approximated by the Guderley-von Kármán axial mass flux:

$$\rho u\cong 1+(1-M_\infty^2)\phi_x-[(\gamma+1)/2]M_\infty^2\phi_x^2 \tag{4}$$

It should be noted that even though the axial velocity is nonzero when Eq. (4) is equal to zero, it will be shown that this does not represent a serious limitation even at stagnation.

The radial mass flux component is approximated by only the first-order linear term, $\rho v\cong v$. This is consistent with the second-order approximation for the axial mass flux, since as M_∞ approaches 1, it is dominated by the quadratic term. Although the arguments lose their validity around the leading edge, a linear cross-flow term obviates the need for rotated differencing and thus simplifies the algorithm. As will be shown, reasonable results can nonetheless be achieved even at the leading edge.

Surface Boundary Conditions

It was assumed for the nacelle surface boundary condition that all solid surfaces are stream surfaces, i.e.,

$$(\rho\mathbf{v}\cdot\mathbf{n})=0 \tag{5}$$

Given a specific contour representation of an axisymmetric body $\bar{R}=\tau f(\bar{x})$, where τ is the thickness ratio of the nacelle, one cannot arbitrarily apply the tangency condition (5) without considering the linearized conservation law used in the solution algorithm.[9,10] When Eq. (5) is viewed in terms of the effective mass-flux components corresponding to Eq. (1), the tangency condition reduces to

$$\frac{dr}{dx}(x,R)=\frac{\dot{m}_r}{\dot{m}_x} \tag{6a}$$

$$\frac{\dot{m}_r}{\dot{m}_x}=\frac{\text{effective radial mass flux}}{\text{effective axial mass flux}}$$

$$=\frac{\phi_r}{1+(1-M_\infty^2)\phi_x-[(\gamma+1)/2]M_\infty^2\phi_x^2} \tag{6b}$$

Equations (6a) and (6b) are now consistent with Eq. (1) and can be called a mass-flux surface boundary condition. Additional improvement in the results can be obtained by applying the mass-flux conditions on the actual surface of the body. This is especially necessary when considering the close interaction of the nacelle and centerbody. For any given power setting, the nacelle internal mass flow will be controlled by the nozzle exit area. Failure to set this area correctly can have a dramatic influence on the global characteristics of the flowfield. A demonstration of this interaction will be given shortly.

The exact surface boundary condition used for this paper is a first-order scheme applied at the nearest mesh point. As such, it required very little coding effort.

The differential equation is solved on a nonuniform Cartesian mesh. Type-dependent differencing is used with a successive live over-relaxation solver (SLOR) algorithm. Far-field boundary conditions that set the perturbation velocity ϕ_x to zero are imposed on upstream and downstream surfaces. A Kutta condition is imposed at the cowl trailing edge, with the jump in potential convected downstream on a line of constant radius.

Pressure Relation

Reduction of the solution into a meaningful representation requires some pressure relation consistent with the differential equation and boundary conditions. Treating the mass flux in the momentum equation in the same fashion as in the continuity equation[9] and integrating along an arbitrary streamline from the reference condition at infinity produces

$$C_p=-2\phi_x-(1-M_\infty^2)\phi_x^2+[(\gamma+1)/3]M_\infty^2\phi_x^3-\phi_r^2 \tag{7a}$$

where the leading term is the basic small disturbance theory contribution and the second the standard higher-order correction term.

Figure 1, however, compares several C_p formulas for a one-dimensional flow. The reference curve (solid line) is the exact C_p formula,

$$C_p=\frac{2}{\gamma M_\infty^2}\left\{\left[1-\left(\frac{\gamma-1}{2}\right)M_\infty^2(|v|^2-1)\right]^{\gamma/(\gamma-1)}-1\right\} \tag{7b}$$

is plotted vs the corresponding exact one-dimensional expression for ρu. The various C_p expressions in combination with the small disturbance mass flux [Eq. (4)] are compared against this standard. It should be noted that the mass flux, whether exact or small disturbance, is used for the abscissa, since it is the quantity conserved by both the differential equation and boundary conditions.

The figure shows that the lower-order C_p formulas ($-2\phi_x$, $-2\phi_x-\beta\phi_x^2$) have a very limited range of applicability. The exact C_p formula vs the small disturbance ρu follows the reference curve quite closely over the entire range of interest. Equation (7a) compares equally well for this one-dimensional example (not shown on Fig. 1); however, the radial terms in Eq. (7a) can yield excessive overexpansions around the leading edge in a two-dimensional flow. The results of two-dimensional calculations are therefore presented with the exact C_p formula.

It should be noted, however, that any drag calculation should use the consistent C_p expression (7) to guarantee zero wave drag in a shock free flow. Following the scheme of Steger and Baldwin[11] results in the following mass-flux form

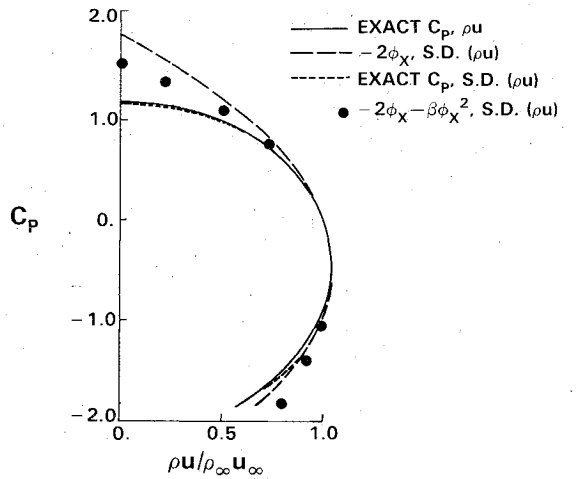

Fig. 1 Quasi-one-dimensional C_p comparison study for $M_\infty = 0.8$.

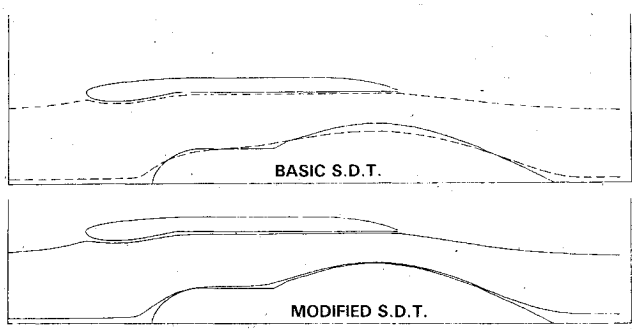

Fig. 2 Streamline comparisons for small disturbance model.

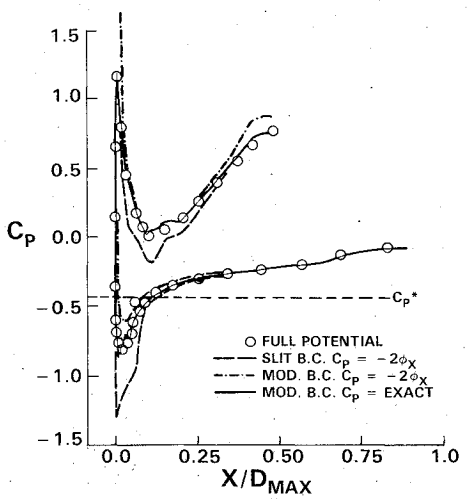

Fig. 3 Comparison of surface boundary condition and C_p models for inlet, $M_\infty = 0.8$.

for the drag

$$\frac{\text{Drag}}{q_\infty} = \int_{\substack{\text{shock}\\ \text{face}}} \left[(1-M_\infty^2)(u_2^2-u_1^2) - \frac{2}{3}(\gamma+1)M_\infty^2(u_2^3-u_1^3) \right] dA \tag{8}$$

Results of Improved Boundary Conditions

The combination of the modified boundary condition (mass flux at the exact surface) with the exact pressure coefficient

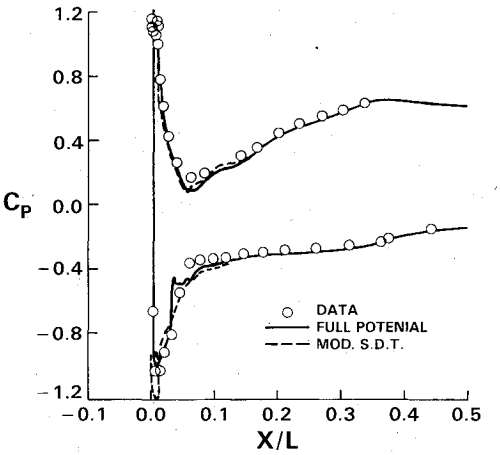

Fig. 4 Pressure coefficient comparisons for advanced inlet design, $M_\infty = 0.795$, MFR = 0.794.

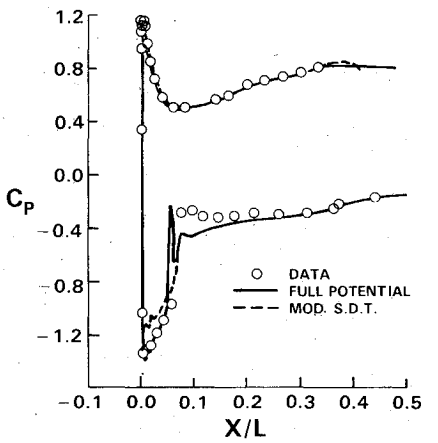

Fig. 5 Pressure coefficient comparisons for advanced inlet design, $M_\infty = 0.798$, MFR = 0.64.

calculation significantly improves the small disturbance theory applicability. This is demonstrated in the following two numerical calculations. The first study shows the failure of the standard small disturbance boundary conditions to correctly establish one of the primary controlling influence on the flowfield, i.e., the nozzle area. (Cowl surface is defined with an exact surface boundary condition in all methods used in this study.) In this example, a nacelle/centerbody through-flow calculation in a $M_\infty = 0.5$ freestream is studied. The nacelle mass flow is set by the nozzle exit flow area. Three different small disturbance schemes can be considered: 1) a basic small disturbance applying slope condition along a slit, 2) a mass-flux boundary condition also applied along a slit, and 3) a mass-flux boundary condition applied on the actual surface (modified scheme). The latter method utilizes the local potential, rather than the slit potential, to evaluate the boundary condition. For the centerbody, the slit is the centerline. Streamline comparisons near the cowl inner surface and the centerbody are given on Fig. 2. The centerbody streamline is dependent on the choice of boundary conditions used and can, in the case of the basic small disturbance scheme,[1] differ significantly from the actual contour shape. This error at the nozzle exit plane effectively modifies the mass flow ratio, and the overall flow solution is quite different.

The second study focuses both on the boundary condition model as well as the pressure relation used. A sting mounted nacelle inlet without centerbody, operating at a typical cruise condition of $M_\infty = 0.8$, MFR = 0.75, is considered next. Comparisons are presented in Fig. 3 against a full potential analysis[12] using an exact C_p calculation. The nonconservative full potential is used as a benchmark to check out the

modifications to a nonconservative small disturbance method. The basic scheme not only overpredicts the leading edge expansion but indicates the existence of a strong shock. The modified approach with an approximate first-order C_p calculation shows significant improvement but predicts too much leading edge recompression near the hilite. Finally, the agreement predicted by combining the modified boundary condition approach with an exact C_p calculation shows excellent agreement with the "exact" calculation. Again, as seen in Fig. 1, the higher-order terms do not contaminate the C_p calculation. It should be noted that all the small disturbance calculations were made on the same grid in an attempt to segregate the known grid dependence of the basic scheme.

This brings out one of the big advantages of the exact surface boundary conditions. Experience indicates that by modifying the grid, the standard small disturbance model can be made to correlate rather well with the data. Exact surface boundary conditions, on the other hand, yield results which are quite insensitive to the grid.

Further proof of the accuracy of this modified approach is shown on Figs. 4 and 5, where pressure coefficient comparisons with experimental data[13] are made on an inlet designed for an advanced transport aircraft. The small disturbance results for both mass flow ratio cases are in substantial agreement with the full potential predictions and the data, with only slight differences being noted, as should be expected, in the hilite region.

Power Addition

The generation of thrust from an engine results from the transfer of power to the ambient air. Though conceptually similar, a ducted fan and a free propeller differ in certain fundamental aspects. A free propeller interacts directly with the freestream so that conditions at the face of a free propeller depend upon both the propeller power setting and the flight Mach number. This is in contrast to the behavior of a ducted fan in which the Mach number at the face of the fan is dependent only on the fan power setting, not on the flight Mach number. These considerations have implications with regard to the computational demands. Thus the fan stream is coupled to the freestream flow rather indirectly through matching conditions across the wake (or slip) discontinuity, whereas the free propellor stream is coupled directly to the freestream flow in the immediate vicinity of the propellor tip.

The enthalpy and axial momentum increases actually provided by a fan or propellor are conveniently represented mathematically by use of the actuator disk concept.[14] The actuator disk simply provides a method for introducing the enthalpy and axial momentum increases as a discontinuous "jump" at the actuator disk. As a result, the effects of the fan or propellor appear only as matching conditions across the disk, and it is not necessary to consider the detailed representation of the blade geometry.

Flow irrotationality is implicity assumed in the governing equation (1) discussed in the previous section through definition of a velocity potential. The problem formulation can retain the convenience of the potential formulation if we restrict our attention to situations where the powered stream as well as the freestream are irrotational. By so doing, the only vorticity present within the field will exist as a singularity on the slip surface joining the exhaust jet to freestream. The entire powered stream is then matched to the freestream through the jump conditions across the actuator disk and along the exhaust jet slip surfaces.

The jump conditions across the actuator disk may be written[15]

$$[\rho u] = 0 \tag{9a}$$

$$[v] = \frac{1}{\rho u}\int_{-\delta}^{\delta} \rho f_r \, dx \tag{9b}$$

In this latter expression, f_r is the volumetric radial force of the blade row, so the integral from $-\delta$ to δ represents the effect of the total radial force of the blade at the given radius. In many applications the radial force of the almost radial blades can be considered small, so for simplicity the radial force contribution is ignored. We thus introduce the approximate matching condition $[v] = 0$.

Prescription of the downstream stagnation pressure and the downstream stagnation temperature allows introduction of the downstream reference Mach number $M_{\infty 2}$, defined as the Mach number existing when the internal flow reaches the ambient static pressure (p_∞). In order to apply the continuity matching condition, Eq. (9a), it is necessary to relate the density to the local velocity and appropriate reference Mach number. Utilization of the mass-flux form of the continuity relationship in Eq. (9a) leads to

$$\dot{m}_x = 1 + (1 - M_{\infty 1}^2)\, u_1 - \left(\frac{\gamma+1}{2}\right) M_{\infty 1}^2 u_1^2$$

$$= A\left[1 + (1 - M_{\infty 2}^2)\, u_2 - \left(\frac{\gamma+1}{2}\right) M_{\infty 2}^2 u_2^2\right] \tag{10a}$$

in which there has been introduced the mass-flux scaling parameter

$$A = \frac{(T_{0_2}/T_{0_1}^{1/2})}{P_{0_2}/P_{0_1}} \cdot \frac{M_{\infty 1}}{M_{\infty 2}} \cdot \left[\frac{1 + [(\gamma+1)/2] M_{\infty 2}^2}{1 + [(\gamma-1)/2] M_{\infty 1}^2}\right]^{(\gamma+1)/2(\gamma-1)} \tag{10b}$$

Equation (10a) is a quadratic equation for u_2, so that an expression for the jump in velocity across the disk follows directly to give

$$[u] = u_2 - u_1 = \frac{1}{(\gamma+1) M_{\infty 2}^2}\left[(1 - M_{\infty 2}^2) - \sqrt{(1 - M_{\infty 2}^2)^2 - 2(\gamma+1) M_{\infty 2}^2 (\dot{m}_x/A - 1)}\right] - u_1 \tag{11}$$

This expression gives u_2 as a function of u_1 and the known upstream and downstream reference conditions. It is to be noted that the negative root was selected to ensure that both the jump in velocity remains zero for an unloaded disk and the velocity u_2 be subsonic. The assumed condition of neglecting radial force effects ($[v] = 0$) can be integrated to show that $[\phi]$ across the disk is zero. These two jump conditions act like a ϕ_{xx} operator and determine ϕ across the disk.

Exhaust Plume/Wake Considerations

Across this "wake" there is a discontinuity in properties which must be accounted for in the solution algorithm. Even in the flow-through situation, where no power transfer occurs, a jump in potential corresponding to the circulation of the nacelle (Kutta condition) must be accounted for. The wake is defined by the boundary streamlines of the coflowing streams, with the potential of each being (ϕ_u, ϕ_L) defined in terms of the direction of approach to the discontinuity. An alternate approach, consistent with the classical application of the Kutta condition, is to define a mean potential $\bar{\phi}$ and a corresponding jump in potential

$$[\phi] = \phi_u - \phi_L \tag{12}$$

Two relationships are needed to determine $\bar{\phi}, [\phi]$. Orienting the equations in a streamwise/normal coordinate system results in

continuity of mass

$$[\rho v_n] = 0 \tag{13a}$$

continuity of pressure

$$[p]=0 \tag{13b}$$

Equation (13a) is equivalent to a condition enforcing continuity of streamline slope, using the effective mass-flux definitions for the upper and lower flow, e.g.,

$$\tan\theta=\left[\frac{\phi_{r_u}}{1+(1-M^2_{\infty 1})\phi_{x_u}-[(\gamma+1)/2]M^2_{\infty 1}\phi^2_{x_u}}\right] \tag{14}$$

Ideally, Eqs. (13a) and)14) should be applied along the separating streamline; but keeping in mind the basic small disturbance philosophy, the auxiliary conditions are imposed instead along a line of constant radius. The flow, however, is not constrained to this path.

Imposing the pressure identity (13b) in terms of the velocity potential requires two Bernoulli equations of the form,

$$p=p_0[1-\{(1-\phi_x)^2+\phi_r^2\}\{1-(p_\infty/p_0)^{(\gamma-1)/\gamma}\}]^{\gamma/(\gamma-1)} \tag{15}$$

The use of p_∞ as the reference condition for all flow regions means that separate reference Mach numbers must be used for the bypass and energized flow in their respective differential equations. The pressure matching results in the following relationship between the bypass and energized velocities:

$$(1+\phi_{x_L})^2+\phi^2_{r_L}=c_1[(1+\phi_{x_u})^2+\phi^2_{r_u}]+c_2 \tag{16a}$$

where

$$c_1=(p_{0_u}/p_{0_L})^{(\gamma-1)/\gamma}[1-(p_\infty/p_{o_u})^{(\gamma-1)/\gamma}] \div[1-(p_\infty/p_{0_L})^{(\gamma-1)/\gamma}] \tag{16b}$$

$$c_2=[(1-(p_{0_u}/p_{0_L})^{(\gamma-1)/\gamma}]/[1-(p_\infty/p_{0_L})^{(\gamma-1)/\gamma}] \tag{16c}$$

Negelecting the ϕ_r^2 term as small (slender wing theory model), Eqs. (16a-c) can be recast in terms of the wake potential jump,

$$\tfrac{1}{4}(1-c_1)[\phi]_x^2-(1+c_1)(1+\bar{\phi}_x)[\phi]_x+(1-c_1)(1+2\bar{\phi}_x+\bar{\phi}_x^2)-c_2=0 \tag{17}$$

The quadratic equation (17) could be solved directly for $[\phi]$; however, such an approach encounters iteration problems as $c\to 1$ (unpowered limit). A standard Newton-Raphson technique is therefore used to determinie $[\phi]_x$ from the trailing edge or turboprop tip, with the appropriate root chosen to generate coflowing flows. The boundary conditions at the downstream "infinity" plane do not require any modification except to account for upwind differencing in a supersonic plume. Since both streams are referenced to the same p_∞, the perturbation velocities in both streams go to zero as the pressure returns to its ambient value of p_∞. Thus at the downstream boundary,

$$\phi_x=\phi_{x_u}=\phi_{x_L}=0$$

The slope condition defines $[\phi]_r$, while the pressure match defines $[\phi]_x$. In contrast to the disk modeling, the jump in ϕ is not zero across the wake.

A second-order accurate scheme defining the flow on each side of the wake introduces image points (ϕ^u,ϕ^L) to make finite differencing of the radial derivatives (ϕ_r,ϕ_{rr}) possible. These additional unknowns require two additional or auxiliary relations to close the system that again can be obtained from "upper" and "lower" versions of Eq. (1).

The effect of power on the jet behavior can be analytically demonstrated by considering the limiting case of small power addition, i.e., $\Delta p_0/p_0 \ll 1$. Taking the lower-order form of Eq. (16a),

$$(1+2\phi_{x_L})=c_1(1+2\phi_{x_u})+c_2$$

and evaluating the limiting forms of c_1,c_2 results in the pressure coefficient expression

$$C_{p_L}=C_{p_u}-\left(\frac{2}{\gamma M^2_\infty}\frac{\Delta p_0}{p_{0_u}}\right)$$

Power addition to the internal stream therefore reduces the local C_p and raises the flow Mach number. The discontinuity in C_p is introduced by using a different reference q_∞ for the internal and external streams (not the definition used in the graphical results, showing C_p continuity).

Powered calculations have been made for the flow-through geometry already examined in Fig. 2. Figures 6 and 7 show Mach number contour plots of the exhausting flow, both with and without power. The ambient Mach number 0.8 and the

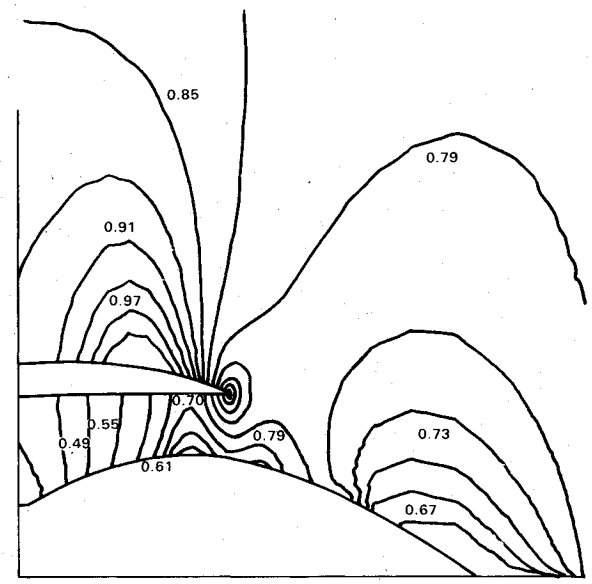

Fig. 6 Mach number contours of afterbody of unpowered flow-through nacelle with convergent-divergent nozzle, $M_\infty = 0.8$.

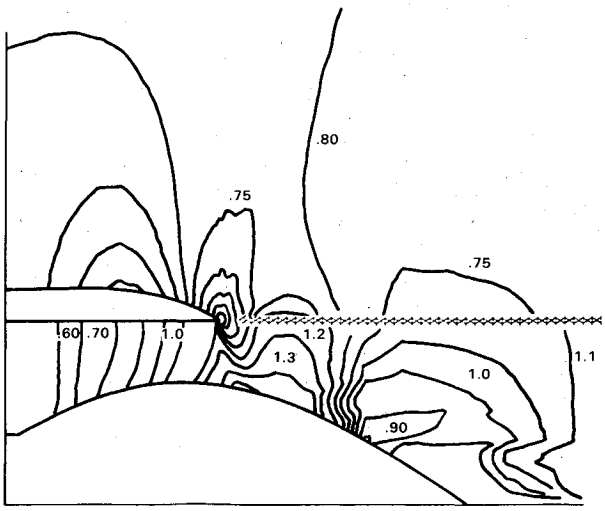

Fig. 7 Mach number contours on afterbody of powered nacelle with convergent-divergent nozzle, $M_\infty = 0.8$, $\Delta P_0/P_0 = 0.5$.

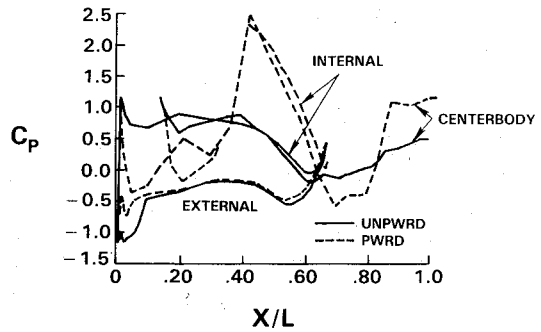

Fig. 8 Pressure coefficient comparisons for both an unpowered and powered nacelle, $M_\infty = 0.8$.

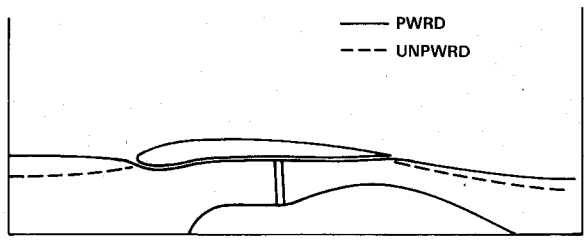

Fig. 9 Effect of power on nacelle stagnation streamline at low speed.

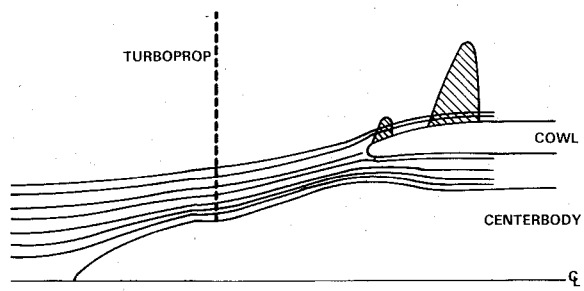

Fig. 10 Geometry and streamlines for turboprop calculation, $M_\infty = 0.8$, $\Delta P_0/P_0 = 0.10$, $\Delta T_0/T_0 = 0.03$.

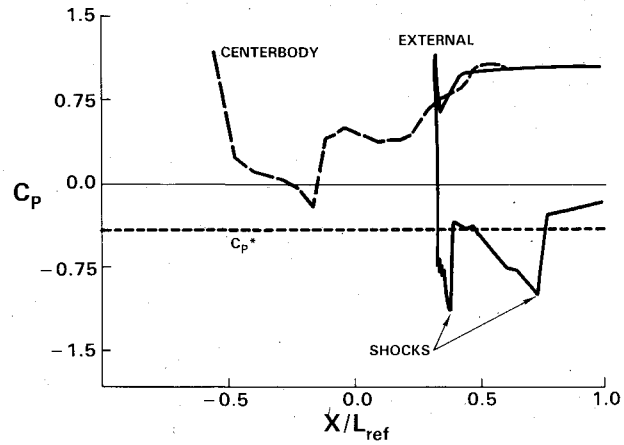

Fig. 11 Pressure coefficient on centerbody and cowl for turboprop configuration, $M_\infty = 0.8$, $\Delta P_0/P_0 = 0.10$, $\Delta T_0/T_0 = 0.03$.

power setting is $p_{02}/p_{01} = 1.5$, $T_{01}/T_{02} = 1.123$. The oblique shock forming off the afterbody trailing edge indicates the powered case is overexpanded ($p_{ex} < p_{loc.amb}$). The alternating compression and expansion zones seen on the afterbody (Fig. 7) are commonly found in powered plug nozzle experiments.[16] Furthermore, Fig. 8 shows that the addition of power produces a decreased acceleration on the external contour, corresponding to the expected increased mass flow into the nacelle. This is graphically seen in the stagnation streamline

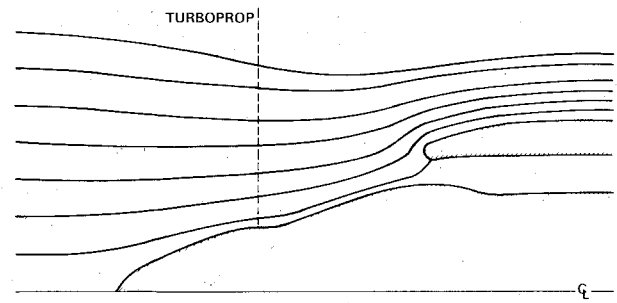

Fig. 12 Demonstration of streamline contraction effect on turboprop configuration at low Mach numbers, $M_\infty = 0.1$, $\Delta P_0/P_0 = 0.05$, $\Delta T_0/T_0 = 0.03$.

calculations shown on Fig. 9. This comparison was made at a lower Mach number to enhance the effect.

The procedure has been applied to the simulation of a turboprop/nacelle interaction, where the centerbody protrudes outside the inlet. The propeller is also modeled by an actuator disk and, for simplicity, the exit flow is assumed to have no swirl. Modifications to the analysis had to be made since in the turboprop case, the wake and propeller share a common origin at the tip, while in the turbofan case the wake dividing the external and energized streams originates off the fan cowl trailing edge. Figures 10 and 11 present streamline plots for a 90% efficient propeller and the corresponding inlet and centerbody pressures. The cross-hatched regions represent local supersonic flow bubbles. The two shocks on the inlet tip cause a total pressure loss and an increase in inlet spillage drag. Even though no tip vortex rollup is modeled, the expected streamtube contraction produced by the disk is obtained (Fig. 12).

Conclusions

An improved small disturbance procedure for modeling nacelles has been formulated. The method utilizes mass-flux boundary conditions consistent with the governing small disturbance equation. These boundary conditions are applied to the actual contour surface. Furthermore, the use of an exact C_p expression is found to improve agreement with true solutions, indicating that the higher-order terms do not contaminate the calculated solution. Finally, the results of this method not only show a substantial agreement with full potential results, but have simulated the global effects of turboprop and turbofan power transfer.

References

[1] Boppe, C.W., "Computational Transonic Flow About Realistic Aircraft Configurations," AIAA Paper 78-104, Hunstville, Ala., Jan. 1978.

[2] Boppe, C.W. and Stern, M.A., "Simulated Transonic Flows for Aircraft with Nacelles, Pylons, and Winglets," AIAA Paper 80-0130, Pasadena, Calif., Jan. 1980.

[3] Shankar, V. and Malmuth, N., "Computational and Simplified Analytical Treatment of Transonic Wing/Fuselage/Pylon/Store Interactions," *Journal of Aircraft*, Vol. 18, Aug. 1981, pp. 631-637.

[4] Ashley, H. and Landahl, M., *Aerodynamics of Wings and Bodies*, Addison-Wesley, New York, 1965, pp. 227-244.

[5] Chin, W.C., "Some Singular Aspects of Three-Dimensional Transonic Flow," *AIAA Journal*, Vol. 16, March 1978, pp. 275-277.

[6] Kuchemann, D. and Weber, J., *Aerodynamics of Propulsion*, McGraw-Hill, New York, 1953, p. 73.

[7] Widnall, S.E. and Barrows, T.M., "An Analytic Solution for Two and Three-Dimensional Wings in Ground Effect," *Journal of Fluid Mechanics*, Vol. 41, pt. 4, 1970, pp. 769-792.

[8] Van der Vooren, J., Slooff, J.W., Huizing, G.H., and Van Essen, A., "Remarks on the Suitability of Various Transonic Small Perturbation Equations to Describe Three-Dimensional Transonic Flow; Examples of Computations using a Fully-Conservative Rotated Difference Scheme," *Transonicum Symposium II*, Gottingen, Germany, Springer-Verlag, N.Y., 1975, .

[9]Schmidt, W., "A Self-Consistent Formulation of the Transonic Small Disturbance Theory," *Recent Developments in Theoretical and Experimental Fluid Mechanics,* Springer-Verlag, New York, 1979, pp. 48-57.

[10]Chin, W.C., "Goethert's Rule with an Improved Boundary Condition," *AIAA Journal,* Vol. 15, Oct. 1977, pp. 1516-1518.

[11]Steger, J.L. and Baldwin, B.S., "Shock Waves and Drag in the Numerical Calculation of Isentropic Transonic Flows," NASA TN D-6997, 1972.

[12]Caughey, D.A., and Jameson, A., "Accelerated Iterative Calculation of Transonic Nacelle Flowfields," *AIAA Journal,* Vol. 15, Oct. 1977, pp. 1474-1480.

[13]Crook, J.L., Nelson, D.P., Wiley, R.H. and Presz, W.M., "Isolated Nacelle Performance-Measurement and Simulation," AIAA Paper 81-0134, Orlando, Fla, Jan. 1982.

[14]Horlock, J.H., *Actuator Disk Theory,* McGraw Hill Book Co., New York, pp. 12-31, 1978.

[15]Oates, G.C., "Through-Flow Theory," *The Aerothermodynamics of Aircraft Gas Turbine Engines,* AFAPL-TR-78-52, Air Force Aero Propulsion Lab., Wright-Patterson AF Base, Ohio, 1978.

[16]Powell, R.D. and Yeates, J.E., "Lift/Cruise Fan Exhaust System Research Program," U.S. Army Transport Research Command, Fort Eustis, Va. TRECOM Tech. Rept. 64-49, 1964.